IEEE Access
Multidisciplinary | Rapid Review | Open Access Journal

Received January 27, 2021, accepted February 8, 2021, date of publication February 16, 2021, date of current version February 24, 2021.

Digital Object Identifier 10.1109/ACCESS.2021.3059700

Theoretical Modeling and Analysis of Circularly Polarized Annular Leaky-Wave Antenna Based on Travelling-Wave Structure

YUCHEN MA AND JUNHONG WANG, (Senior Member, IEEE)
Key Laboratory of all Optical Network and Advanced Telecommunication Network of Ministry of Education, Beijing Jiaotong University, Beijing 100044, China
Corresponding author: Junhong Wang (wangjunh@bjtu.edu.cn)

This work was supported in part by the National Nature Science Foundation of China (NSFC) Project under Grant 62031004 and Grant 61871025.

ABSTRACT In this paper, a theoretical model based on the electric field integration method is proposed to analyse radiation properties of the slotted annular Leaky-Wave Antenna (LWA), which can generate a Circularly Polarized (CP) conical beam or broadside beam. The annular LWA contains radiating elements arranged along a circular travelling-wave structure with equal intervals. By combining the proposed model and LWA theory, the design procedure for the annular SIW LWA is presented. To verify the model, three examples of LWAs with different beam angles have been designed and fabricated. Calculation results from the proposed model are consistent with the simulation and measurement results. The model can significantly reduce the design period and is an instructive tool for antenna design.

INDEX TERMS Theoretical model, leaky-wave antenna, conical and broadside beam, circular polarization, annular travelling-wave structure.

I. INTRODUCTION

Circularly polarized (CP) conical beam antennas have been studied for a long time and attract increasing attention due to their low polarization mismatch loss, especially in satellite communication. Several types of methods have been proposed to generate the CP conical beam. One type of methods is to excite high-order modes. In [1], a dual-CP microstrip antenna with a conical beam is proposed by exciting the second-order mode. In [2], a pattern-reconfigurable antenna is proposed, which generates a broadside beam by the TM_{11} mode and a conical beam by exciting the TM_{21} mode. Another type of methods is to simultaneously excite two orthogonal modes. In [3], a CP conical beam array antenna with polarization diversity is designed by controlling PIN diodes and generating two orthogonal modes. In [4], by exciting two orthogonal modes (TM_{01} and TE_{01}) in a circular aperture, a CP conical beam antenna is realized. In [5], a CP conical beam is produced by simultaneously exciting the loop mode and monopole mode using a patch antenna, and it switches between right-hand CP and left-hand CP beams by PIN diodes. In [6], by exciting two modes (TM_{01} and TM_{02}), a wideband CP conical beam antenna is designed. In [7], a CP conical beam antenna is proposed by a circular-monopolar patch surrounded with eight reconfigurable stubs, and the left- and right-hand CP are switched by PIN diodes. In [8], a low-profile CP antenna with a conical-beam pattern is presented, which contains a monopolar patch surrounded by ring-shaped parasitic elements. In [9], a novel CP conical-beam antenna with horizontal and vertical radiators around a monopole is proposed, whose beam angle is tuned by the height of parasitic elements. In [10], a wideband CP conical-beam microstrip antenna with a large ground plane is designed. In [11], a CP conical beam antenna that consists of a feeding probe and a parasitic dielectric parallelepiped element is proposed. In [12], a low-profile substrate integrated waveguide (SIW) antenna with a CP conical beam is designed by combining a radial current source and a loop current source. In addition to these two types of methods, a CP conical beam can be generated by a CP array using CP radiation elements, e.g., in [13], orthogonal slots are notched on a metallic truncated circular

The associate editor coordinating the review of this manuscript and approving it for publication was Chan Hwang See.

cone to generate a CP conical beam pattern. As a new method, a torus knot antenna with a CP conical beam is proposed by generating an annular current [14].

Most of the mentioned designs are based on standing-wave structures. Studies on CP conical-beam antennas designed based on travelling-wave structures are less comprehensive. In [15], a wideband two-arm spiral antenna producing a CP conical beam is proposed. In [16], a CP conical beam is generated by a low-profile two-arm Archimedean spiral antenna. In [17], a leaky-wave antenna with switchable omnidirectional conical radiation by frequency is proposed. These designs have continuous current distributions. In fact, by arranging radiating elements along a circle travelling-wave structure, it is possible to generate CP conical or broadside beams. In [18], a series-fed circular patch array that generates a broadside beam is designed using coplanar proximity coupling, which presents the merit of a low-profile structure with a single layer. In [19], a series-fed square patch array for broadside beam radiation is designed, which is fed by a circular meandered microstrip transmission line beneath the radiating layer. Meanwhile, a theoretical model for the series-fed antenna array is proposed in [19], which uses the far field of one unit as initial data to analyse the axial ratio of the entire array.

As a typical type of antennas, Leaky-Wave Antennas (LWAs) can be constructed by different types of transmission lines such as microstrip line [20] and SIW [21]. In [20], a microstrip line working on pin-loaded EH1-mode is proposed, which effectively extends the distance of in-phase equivalent magnetic-current line sources for gain enhancement. For the SIW, a simple structure makes it easily fabricated on a printed circuit board and realizes the low-profile LWA [22].

In this paper, a theoretical model for slotted annular LWAs based on travelling-wave structures is introduced. Unlike that in [19], the proposed model uses field distribution in the slot aperture to analyse the far-field pattern and axial ratio of the array. Two types of beam patterns (broad side and conical beams) and their axial ratios are investigated. The design guidelines of the array are provided to obtain the desired beam. Furthermore, combining the proposed model with the SIW LWA theory, the design approach for the annular SIW LWA is provided, and relative equations are presented. In the remainder of the paper, the radiation mechanism, modelling procedure and analysis of the CP annular LWA are presented in Section II. The proposed model is validated in Section III. Conclusions are drawn in Section IV.

II. MODELLING AND RADIATION PROPERTY ANALYSIS OF THE ANTENNA

In this section, a 12-element annular travelling-wave slotted antenna array is first modelled and analysed to explain the radiation mechanism, including the CP principle of this type of antenna array. Then, a theoretical model for the CP conical-beam LWA is established using the electric field integration method. Finally, the radiation properties of the antenna are analysed.

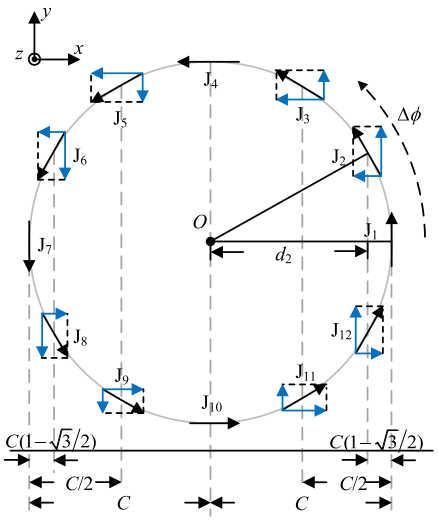

FIGURE 1. Schematic diagram of the 12-element annular array.

A. RADIATION MECHANISM OF ANNULAR LWA

Fig. 1 shows the case of a 12-element antenna array, where each element is represented by a current element. For simplicity, all elements are assumed to have equal amplitudes. In the annular array, the phase variation of the travelling wave is set as 4π. In Cartesian coordinate system, each current element is decomposed into x and y components, i.e., J_{xm} and J_{ym} components. To calculate the far field pattern in the xoz-plane, E_θ is derived from J_x, E_φ is derived from J_y, and they are expressed by

$$E_\theta(\theta) = \frac{e^{-jkr}}{r}(I_{x_1}e^{-j(\phi_{x_1}+kd_1\sin(\theta))} + I_{x_2}e^{-j(\phi_{x_2}+kd_2\sin(\theta))} \cdots + I_{x_{12}}e^{-j(\phi_{x_{12}}+kd_{12}\sin(\theta))}) \quad (1)$$

$$E_\varphi(\theta) = \frac{e^{-jkr}}{r}(I_{y_1}e^{-j(\phi_{y_1}+kd_1\sin(\theta))} + I_{y_2}e^{-j(\phi_{y_2}+kd_2\sin(\theta))} \cdots + I_{y_{12}}e^{-j(\phi_{y_{12}}+kd_{12}\sin(\theta))})\cos\theta \quad (2)$$

where I_{x_m}, I_{y_m}, ϕ_{x_m} and $\phi_{y_m}$are the amplitude and phase of components J_{xm} and J_{ym}, as listed in Table 1; r is the distance between an observation point and centre point O; d_m is the projection of the position vector of each element; k is the propagation constant in free space. An additional π is added in ϕ_{x_m} and ϕ_{y_m} due to the rotation of the element, as shown in Table 1. To obtain the left- and right-hand circular polarization (LHCP and RHCP) components, the expressions are

$$\boldsymbol{E}_{\mathrm{L}} = (\boldsymbol{E}_\theta + \mathrm{j}\boldsymbol{E}_\varphi)/\sqrt{2} \quad (3)$$

$$\boldsymbol{E}_{\mathrm{R}} = \left(\boldsymbol{E}_\theta - \mathrm{j}\boldsymbol{E}_\varphi\right)/\sqrt{2} \quad (4)$$

Moreover, the axial ratio is expressed by

$$\mathrm{r_A} = \frac{E_{\mathrm{L}} + E_{\mathrm{R}}}{E_{\mathrm{L}} - E_{\mathrm{R}}} \quad (5)$$

TABLE 1. Element information of the 12-element circular array.

Ele.(m)	I_{x_m}	I_{y_m}	ϕ_{x_m}	ϕ_{y_m}	Pos.(C)
1	0	1	0	0	(1,0)
2	1/2	$\sqrt{3}/2$	$-\pi/3$	$-\pi/3$	($\sqrt{3}$,1/2)
3	$\sqrt{3}/2$	1/2	$-2\pi/3$	$-2\pi/3$	(1/2, $\sqrt{3}$)
4	1	0	$-\pi$	$-\pi$	(0,1)
5	$\sqrt{3}/2$	1/2	$-4\pi/3$	$-4\pi/3+\pi$	(-1/2, $\sqrt{3}$)
6	1/2	$\sqrt{3}/2$	$-5\pi/3$	$-5\pi/3+\pi$	(-$\sqrt{3}$,1/2)
7	0	1	0	π	(-1,0)
8	1/2	$\sqrt{3}/2$	$-\pi/3+\pi$	$-\pi/3+\pi$	(-$\sqrt{3}$,-1/2)
9	$\sqrt{3}/2$	1/2	$-2\pi/3+\pi$	$-2\pi/3+\pi$	(-1/2,-$\sqrt{3}$)
10	1	0	$-\pi+\pi$	0	(0,-1)
11	$\sqrt{3}/2$	1/2	$-4\pi/3+\pi$	$-4\pi/3$	(1/2,-$\sqrt{3}$)
12	1/2	$\sqrt{3}/2$	$-5\pi/3+\pi$	$-5\pi/3$	($\sqrt{3}$,-1/2)

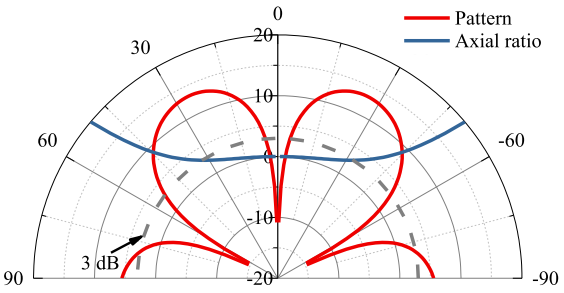

FIGURE 2. RHCP pattern and axial ratio of the 12-element circular array in the *xoz*-plane.

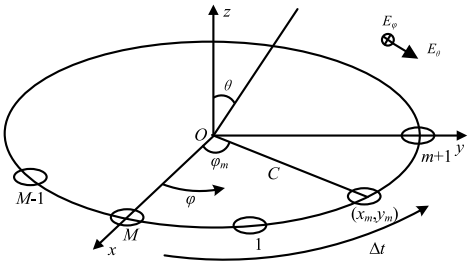

FIGURE 3. Spatial model of the travelling-wave slotted circular array.

The radius of array R is set to 0.62 λ, where λ is the wavelength in free space. The RHCP component pattern and axial ratio of the wave in the upper *xoz*-plane can be obtained, as depicted in Fig. 2. The RHCP conical beam, which points to 26° is generated by the annular LWA, and the axial ratio is less than 3 dB in the range of (−33°, 33°). This result explains the generation of CP properties and can produce a conical beam pattern. When the travelling wave is anticlockwise, the polarization is RHCP. Conversely, LHCP can be generated by a clockwise travelling wave.

B. MODELLING

The proposed travelling-wave slotted annular antenna array to generate a CP conical beam is depicted in Fig. 3, where

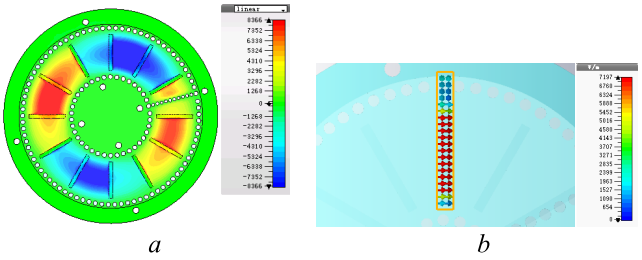

FIGURE 4. Electric distributions of (a) the waveguide and (b) a slot aperture.

radiating elements are arranged along a circle with constant interval. Each element corresponds to an angle φ_m defined by its position vector and x-axis, where $m = 1, 2, 3, \ldots, M$. Here, it is assumed that the direction of the travelling wave is anticlockwise, as mentioned in the former part, and RHCP is generated. Each adjacent element in the anticlockwise direction has a phase delay of Δt, which should be considered in the calculation of the radiation pattern of the array. The proposed model can predict the radiation properties of the annular LWA, when radius C, wavelength number n and element number M are determined.

Using the equivalence principle, the radiation of each element can be equivalent to that of electric and magnetic currents J and J_m in free space [23], which are

$$\boldsymbol{J} = \hat{n} \times \boldsymbol{H} \tag{6}$$

$$\boldsymbol{J_m} = -\hat{n} \times \boldsymbol{E} \tag{7}$$

where $\boldsymbol{E}$ and $\boldsymbol{H}$ are the field distribution surrounding the slot aperture. For simplicity, a rectangular slice is employed above a slot for 0.15 mm to substitute the closed surface surrounding the slot, as illustrated in Fig. 4(b). The slice covers the majority field of the slot, and the field attenuates by large at the edges of the slice. Thus, the remainder of the field can be omitted. Formulas (6) and (7) can be further expressed by

$$\boldsymbol{J} = -\hat{x}H_y + \hat{y}H_x \tag{8}$$

$$\boldsymbol{J_m} = \hat{x}E_y - \hat{y}E_x \tag{9}$$

The far field of the array can be expressed by

$$E_\theta(\theta, \varphi) = \sum_{m=1}^{M} {E_\theta}^m(\theta, \varphi) e^{-\mathrm{j}\phi_m} \tag{10}$$

$$E_\varphi(\theta, \varphi) = \sum_{m=1}^{M} {E_\varphi}^m(\theta, \varphi) e^{-\mathrm{j}\phi_m} \tag{11}$$

where ${E_\theta}^m$ and E_φ^m are the θ and φ electric field components of the mth element, and

$$\phi_m = (m-1) \times \frac{2n\pi}{M}, \quad m = 1, 2, \ldots, M \tag{12}$$

where $2n\pi$ is the phase variation of the entire waveguide. Assuming a uniform amplitude distribution of field in slots, we obtain the total far field of the annular LWA from one single element by rotating it to different places and summing

up the far field together. Therefore, (10) and (11) can be expressed by

$$E_\theta(\theta,\varphi) = \sum_{m=1}^{M} E_{\theta s}(\theta, \varphi-(m-1)\varphi_s)e^{-\mathrm{j}\phi_m} \quad (13)$$

$$E_\varphi(\theta,\varphi) = \sum_{m=1}^{M} E_{\varphi s}(\theta, \varphi-(m-1)\varphi_s)e^{-\mathrm{j}\phi_m} \quad (14)$$

where $E_{\theta s}$ and $E_{\varphi s}$ are the far field of a single element and are expressed by

$$\begin{aligned} E_{\theta s} = & \begin{pmatrix} -\frac{\mathrm{j}\omega\mu}{4\pi}\int_S^{J_x} GdS' - \frac{1}{4\pi}\int_S J_{my}\frac{\partial G}{\partial z}dS' \\ -\frac{\mathrm{j}}{4\pi\omega\varepsilon}\int_S (J_x\frac{\partial^2 G}{\partial x^2} + J_y\frac{\partial^2 G}{\partial x\partial y})dS' \end{pmatrix} \\ & \times \cos\varphi\cos\theta \\ & + \begin{pmatrix} -\frac{\mathrm{j}\omega\mu}{4\pi}\int_S^{J_y} GdS' - \frac{1}{4\pi}\int_S J_{mx}\frac{\partial G}{\partial z}dS' \\ -\frac{j}{4\pi\omega\varepsilon}\int_S (J_x\frac{\partial^2 G}{\partial x\partial y} + J_y\frac{\partial^2 G}{\partial y^2})dS' \end{pmatrix} \\ & \times \sin\theta\cos\varphi \\ & + \begin{pmatrix} -\frac{1}{4\pi}\int_S (J_{my}\frac{\partial G}{\partial x} - J_{mx}\frac{\partial G}{\partial y})dS' \\ -\frac{\mathrm{j}}{4\pi\omega\varepsilon}\int_S (J_x\frac{\partial^2 G}{\partial x\partial z} + J_y\frac{\partial^2 G}{\partial y\partial z})dS' \end{pmatrix}\sin\theta \end{aligned} \quad (15)$$

$$\begin{aligned} E_{\varphi s} = & \begin{pmatrix} -\frac{\mathrm{j}\omega\mu}{4\pi}\int_S^{J_x} GdS' - \frac{1}{4\pi}\int_S J_{my}\frac{\partial G}{\partial z}dS' \\ -\frac{\mathrm{j}}{4\pi\omega\varepsilon}\int_S (J_x\frac{\partial^2 G}{\partial x^2} + J_y\frac{\partial^2 G}{\partial x\partial y})dS' \end{pmatrix}\sin\varphi \\ & - \begin{pmatrix} \frac{\mathrm{j}\omega\mu}{4\pi}\int_S^{J_y} GdS' - \frac{1}{4\pi}\int_S J_{mx}\frac{\partial G}{\partial z}dS' \\ -\frac{\mathrm{j}}{4\pi\omega\varepsilon}\int_S (J_x\frac{\partial^2 G}{\partial x\partial y} + J_y\frac{\partial^2 G}{\partial y^2})dS' \end{pmatrix}\cos\varphi \end{aligned} \quad (16)$$

where $G = e^{-jkR}/R$; $R = |\boldsymbol{r}-\boldsymbol{r}'|$; $\boldsymbol{r}$ and $\boldsymbol{r}$' are the position vectors of the field point and source point, respectively; $\theta_s = 2\pi/M$ is the angular interval between elements.

The left- and right-hand circular polarization components (LHCP and RHCP) E_L and E_R and the axial ratio can be obtained by equations (3)-(5). Thus, by utilizing the aperture field of a single element, we can obtain the total field of an M-element annular LWA.

C. ANALYSIS OF RADIATION PROPERTIES

In this part, the radiation properties of the annular LWA are analysed based on the proposed model. A rectangular-slotted annular LWA based on SIW is employed as an example [24]. As shown in Fig. 4(a), the SIW only enables the TE_{10} mode excited in it. The interval of metallic vias is arc length s in the circular SIW, so we can use the design criterion $s/d < 2.5$ and $d/w < 1/8$ in [21] to design the circular SIW. The field distribution in the slot aperture is obtained by the full-wave simulation of CST, as illustrated in Fig. 4(b), which has considered the coupling between elements.

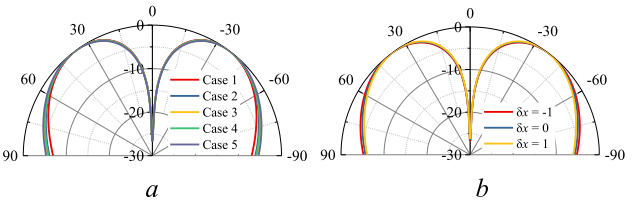

FIGURE 5. Radiation pattern of the slot with (a) different dimensions and (b) different placements.

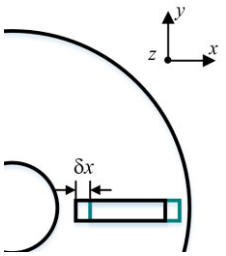

FIGURE 6. Schematic diagram of the slot placement.

TABLE 2. Slot cases of different dimensions.

Case	1	2	3	4	5
slotw	1.2	1.7	2.2	1.2	1.2
slotl	12	12	12	8	10

In the beginning, the effect of the slot sizes and placement on the radiation pattern of the array is studied, and the results are shown in Fig. 5. During the investigation, radius C of the array is set to 21 mm, element number M is set to 12, and guided wavelength number n is set to 2. Table 2 lists five cases of slots with different sizes. As observed in Fig. 5(a), there is no evident difference between the beams, especially for the beam angles in the φ-plane. For the placement effect of the slot as depicted in Fig. 6, a small deviation of δx along the x direction is introduced. The results in Fig. 5(b) show that the slot placement have no significant effect on the radiation patterns. Hence, the radiation pattern of the array is not sensitive to the dimensions and placement of the slots.

The effects of three main parameters on the radiation properties are investigated: radius C, elements number M and wavelength number n. Figs. 7-9 illustrate the radiation properties of the annular LWAs with different C, M and n. The operating frequency is set to 5.8 GHz; C and M are set to 21 mm and 12 when n changes; n and M are set to 2 and 12 when C changes; n and C are set to 2 and 21 mm when M changes.

The radiation patterns in Fig. 7 and 8 are drawn by the co-polarization component, i.e., the RHCP component. In Fig. 7 (a), with increasing n, the beam deviation increases because the phase difference between adjacent elements increases. $n = 1, 2, 3$ correspond to $\theta = 0°$, $36.8°$, $59.1°$ respectively. When n is equal to 1, a broadside beam occurs as illustrated in Fig. 10(a), which implies that the small

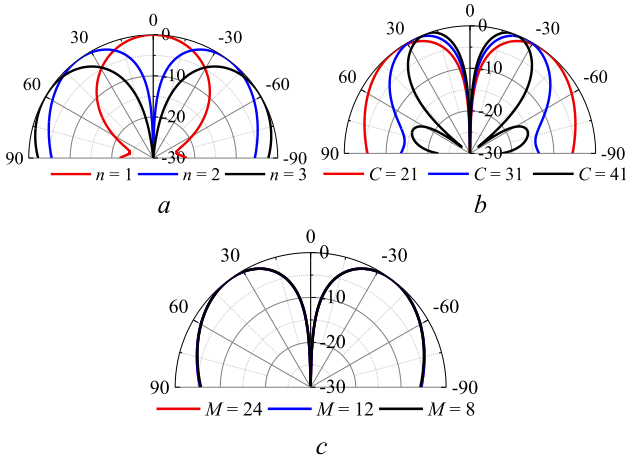

FIGURE 7. Calculated radiation patterns of the LWAs in the *xoz*-plane with different structural parameters: (a) different *n*; (b) different *C*; (c) different *M*.

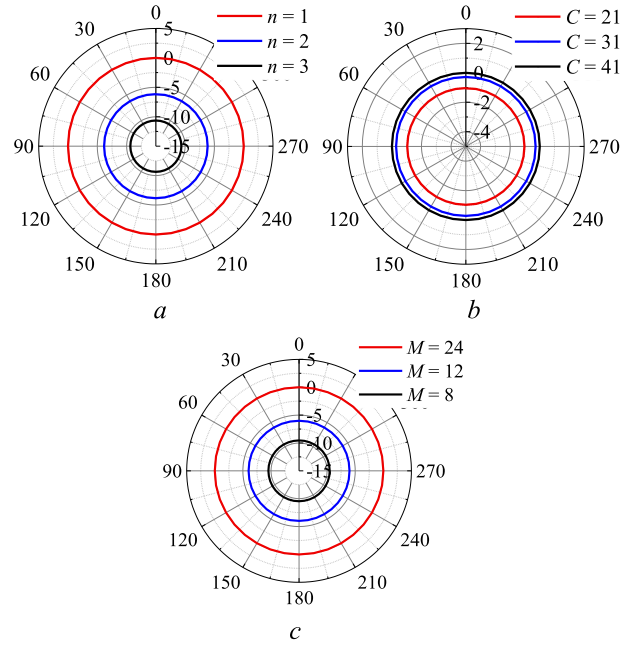

FIGURE 8. Calculated radiation patterns of the LWAs along the conical beam contours with different structural parameters: (a) different *n*; (b) different *C*; (c) different *M*.

phase delay between adjacent elements will let the beams merge to form a zero beam angle. As a demonstration of the conical beam, the 3-D radiation pattern with $n = 2$ is shown in Fig. 10(b). The axial ratio in Fig. 9 (a) increases when the beam deviation increases, due to the increase in LHCP component when θ increases. For $C = 21$ mm, 31 mm and 41 mm, the beam deviation gradually decreases ($\theta = 36.8°$, 26.6°, 20.5°), as shown in Fig. 7 (b), due to the increase in element interval. Radius C hardly affects the axial ratio, as shown in Fig. 9 (b). For $M = 24$, 12, 8, the beam deviation has no obvious change, as shown in Fig. 7 (c), which can be explained by the leaky wave theory [26], i.e., for a fixed phase constant β, the beam angle of the fundamental wave of

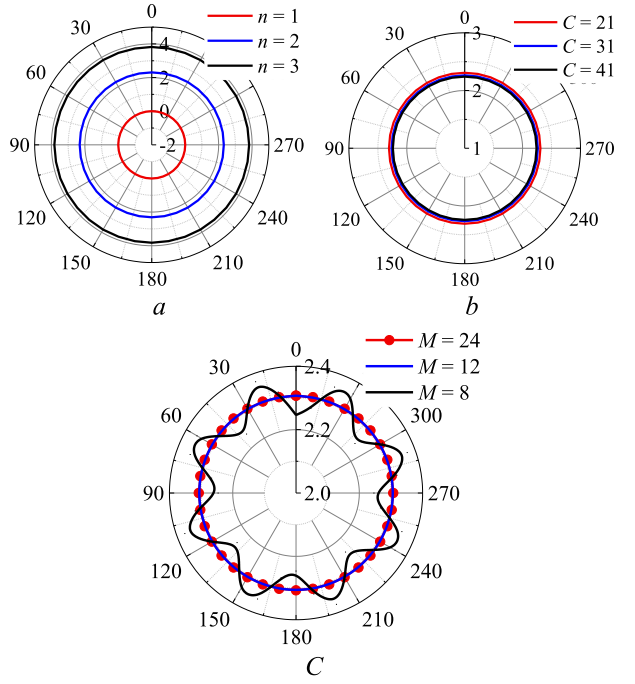

FIGURE 9. Calculated axial ratio of the LWAs along the conical beam contours with different structural parameters: (a) different *n*; (b) different *C*; (c) different *M*.

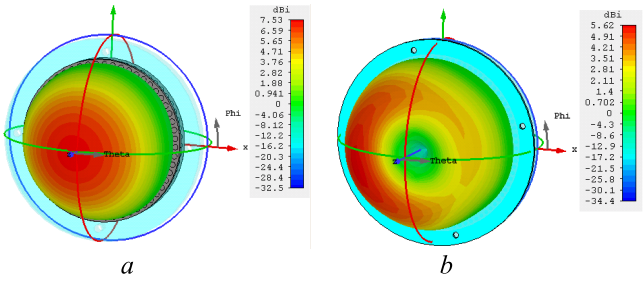

FIGURE 10. 3D far-field radiation patterns of the LWAs: (a) broadside beam pattern; (b) conical beam pattern.

the TE_{10} mode remains constant, which is independent of M. However, when M is small, the axial ratio fluctuates along the beam contour as shown in Fig. 9 (c) because the slots are not sufficiently compactly employed.

For a uniform amplitude distribution of the slot aperture, the radiation pattern is rotationally symmetric for different structural parameters, as depicted in Fig. 8. However, due to the leaky-wave effect in the travelling wave antenna, the amplitudes of elements gradually decrease from the beginning to the end. Hence, it is necessary to study the effect of attenuation constant α on the radiation property. As we know, radiation efficiency η is closely related to α. Thus, for given η and C, α can be obtained by

$$\alpha = -\ln(|S_{21}|/\sqrt{1-|S_{11}|^2})/L \tag{17}$$

$$\eta = 1 - |S_{11}|^2 - |S_{21}|^2 \tag{18}$$

where $L = 2\pi C$. Here, we assume that $|S_{11}|$ is equal to zero. The RHCP radiation pattern and axial ratio with different

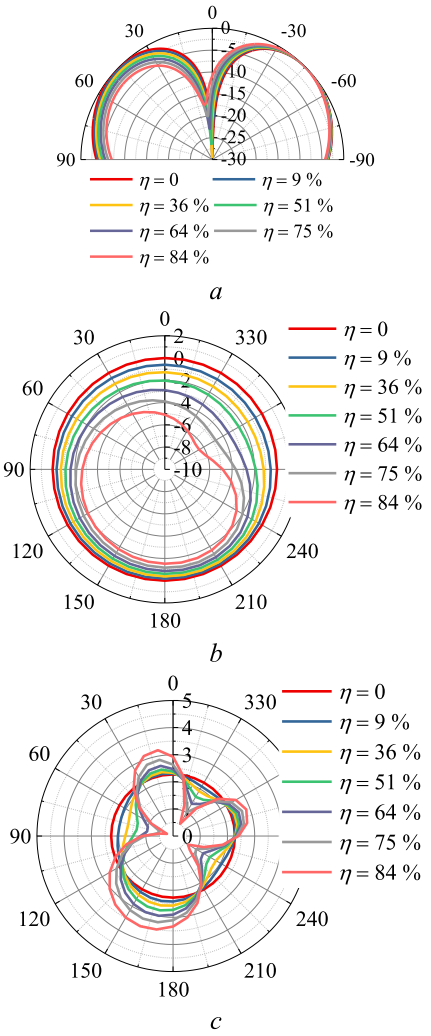

FIGURE 11. Radiation characteristics of LWAs with different radiation efficiencies: (a) radiation pattern in the *xoz*-plane; (b) radiation pattern along the conical beam contour; (c) axial ratio along the conical beam contour.

radiation efficiencies are illustrated in Fig. 11, when C, n and M are set to 2, 14 mm and 12, respectively. In Fig. 11 (a), with increasing η, the conical beam becomes asymmetric. Likewise, the RHCP pattern and axial ratio along the beam contour become twisted. In this case, we can deduce that to guarantee a small variation (less than 3 dB), η should be adequately determined.

D. DESIGN PROCEDURE OF ANNULAR LWA

The previous section shows that the proposed model can be used to predict the radiation properties of the annular array well. Here, the design procedure of the annular array is summarized in Fig. 12 and explained as follows:

1. Selecting the polarization: for RHCP, the travelling wave is anti-clockwise along the structure; for LHCP, the travelling wave is clockwise instead. These selections correspond to the phase delay direction of radiating elements along the structure.

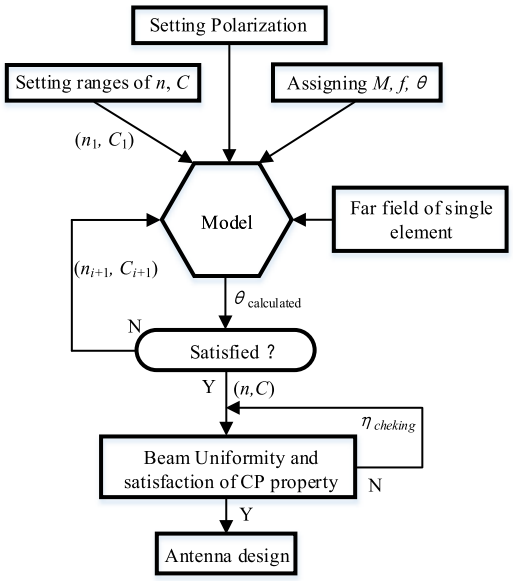

FIGURE 12. Flow diagram of the antenna design based on the proposed model.

2. Assigning the desired beam angle and determining element number M and operation frequency f. Then, calculating the far field of a single magnetic current.
3. Setting the ranges of n and C and constructing a series of (n_i, C_i). Substituting the first pair of (n_1, C_1) and the corresponding far field of the single magnetic current into the proposed model. Comparing the calculated beam angle with the desired beam angle. If the difference between them exceeds the angle tolerance, substituting the next pair of (n_{i+1}, C_{i+1}) into the model for recalculation.
4. Once the pair of (n, C) that yields a satisfying result is obtained, considering η to guarantee the uniformity of the conical beam and CP property. Finally, designing the antenna structure based on the given parameters.

III. DESIGN OF ANNULAR LWA AND EXPERIMENTAL VERIFICATION

To validate the proposed model, three examples of LWAs, i.e., two conical beam LWAs and one broadside beam LWA, are designed and fabricated. Experiments are performed, and the results from the proposed model, full-wave simulation and measurement are compared.

A. DESIGN AND FABRICATION

First, the parameters of the antenna structures are determined. Fig. 13 illustrates the antenna geometry, which is one type of uniform slotted LWA based on the SIW, fed by a coupled aperture. The radiation layer adopts the structure in [24]. The feeding structure contains two rectangular resonance cavities. However, the rectangular structure deteriorates the field uniformity. Hence, the rectangular structure is modified to an arc-shaped structure, as observed in Figs. 13 (c) and (d). The operating frequency is set to 5.8 GHz. Using the proposed

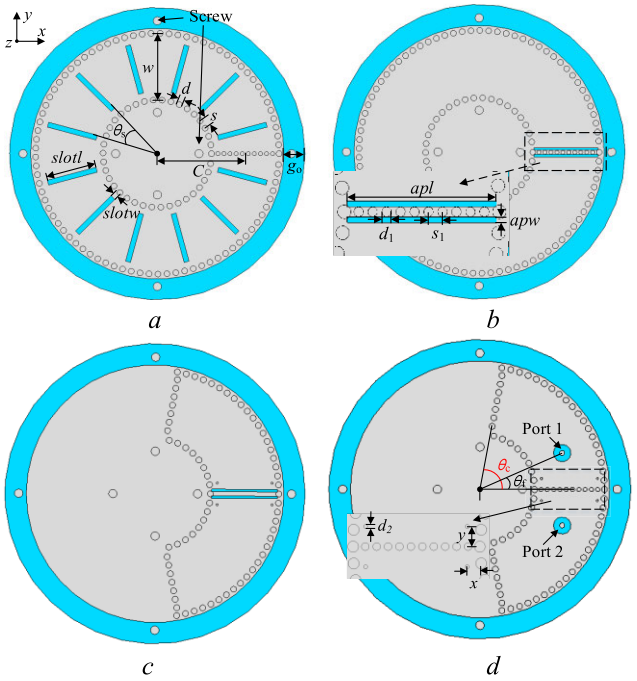

FIGURE 13. Configuration of the proposed LWA: (a) top view of the radiation layer; (b) back view of the radiation layer; (c) top view of the feeding layer; (d) back view of the feeding layer.

model, n and C of the LWAs with desired beam angles can be determined.

The effective permittivity in the SIW can be expressed by

$$\varepsilon_g = \varepsilon_r - (\lambda_0/\lambda_c)^2 \tag{19}$$

where $\varepsilon_r$is the permittivity of the substrate, λ_0 is the wavelength in free space, $\lambda_c = 2w_{eff}$ is the cutoff wavelength, and w_{eff} is the equivalent width of the rectangular waveguide. The propagation constant in the SIW is expressed by

$$\beta = k_0\sqrt{\varepsilon_g} \tag{20}$$

and the relationship between wavelength number n and β is

$$n = \beta L/2\pi \tag{21}$$

where $L = 2\pi C$. Thus, combining equations (19)-(21), we have

$$n = k_0 C\sqrt{\varepsilon_r - (\lambda_0/\lambda_c)^2} \tag{22}$$

where $k_0 = 2\pi/\lambda$. Finally, the relationship between w_{eff}, n and C is obtained by

$$w_{eff} = \frac{\lambda_0/2}{\sqrt{\varepsilon_r - [n/(k_0 C)]^2}} \tag{23}$$

Therefore, from the determined parameters n and C, w_{eff} can be directly calculated by equation (23).

Three LWAs with different beam angles are designed and fabricated. The structural parameters are listed in Table 3. The LWAs are designed on an F4BM-2 substrate with $\varepsilon_r = 3.2$ and $\tan\delta = 0.002$. The thicknesses of the radiation layer and feeding layer are denoted as h_1 and h_2, respectively. The prototypes of the LWAs are shown in Fig. 14. For simplicity, only the feeding layer of LWA 1 is presented, as shown in Figs. 14 (b) and (c). The two-layer LWAs are assembled using plastic screws through four holes drilled along the substrate margins. The LWAs are excited by coaxial probes.

TABLE 3. Structural parameters of the three LWAs.

LWA	C	w	x	y	apl	θ_f	θ_c
1	11.3	15.8	1.5	1.4	15	36°	147°
2	21	16.1	1.6	2.65	15.5	24°	79°
3	14	16.6	1.5	1.9	14	28.6°	102°
s	d	g_o	θ_s	$slotl$	$slotw$	apw	d_1
2.1	1.4	5	30°	12	1.2	0.6	1
s_1	d_2	h_1	h_2				
1.5	0.5	1	3				

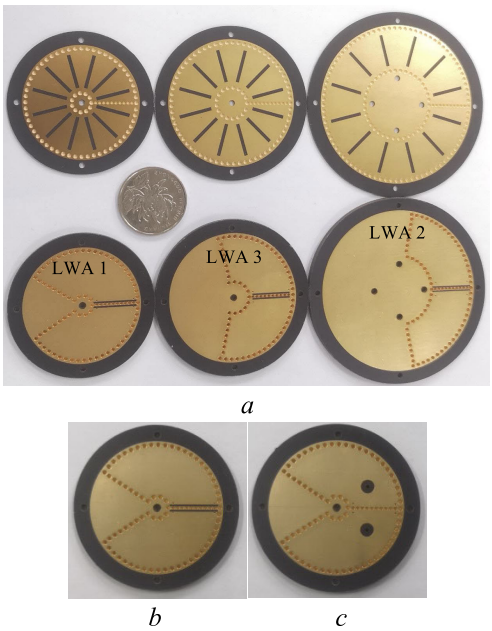

FIGURE 14. Prototypes of the LWAs: (a) top view and back view of the radiation layer of LWA 1, 2 and 3; (b) top view of the feeding layer of LWA 1; (c) back view of the feeding layer of LWA 1.

In an actual LWA, if phase constant β is kept constant, a larger radius C corresponds to larger n. For a fixed-dimension slot and fixed C, a larger element number M causes more leakage, and the attenuation constant α will increase, which may cause a slight perturbation to n, but it can be omitted as usual. In the theoretical model, C, M, and n are independently assigned.

B. MEASUREMENT

Measurements are implemented by the Agilent E8363C PNA network analyser in an anechoic chamber. Fig. 15 shows the $|S|$-parameters of the three LWAs. As shown in Fig. 15, the measurement results are basically consistent with the simulation results. Their differences are mainly caused by the assembling tolerance because a small gap between

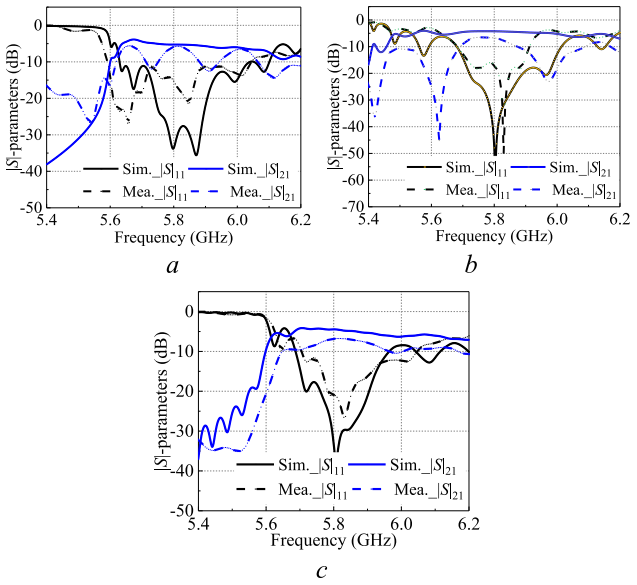

FIGURE 15. |*S*|-parameters of the LWAs, (a) LWA 1, (b) LWA 2, (c) LWA 3.

TABLE 4. Beam angles and gains of the three LWAs.

LWA	Plane	Sim. gain (dB)	Mea. gain (dB)	Sim. beam pointing	Cal. beam pointing	Mea. beam pointing
1	*xoz*	2.15	2.03	35.8°	35.1°	33.9°
1	*yoz*	0.74	0.70	36.4°	35.8°	33.8°
2	*xoz*	0.78	0.62	43.5°	43.7°	43.5°
2	*yoz*	0.14	0.1	45.7°	46°	46.5°
3	*xoz*	3.9	3.71	2.2°	0.1°	4.2°
3	*yoz*	3.9	3.68	2.4°	0.2°	0.77°

radiation and feeding layers appears during assembling processes. Meanwhile, the impedances of the LWAs slightly change from the desired values during the welding procedure of the coaxial connecters.

Fig. 16 shows the normalized radiation patterns of the three LWAs. The calculation results of the proposed model are basically consistent with the simulation and measurement results. The discrepancies between the measurement results and the other two results are partly attributed to the measurement tolerance. Meanwhile, the use of the rectangular field extractor introduces tolerance. The effect of the edge and field in back of the structure are not calculated. Otherwise, due to the use of the planar equivalent principle, the proposed model is only suitable for the upper half space of the antenna. The gains and beam angles in two perpendicular planes of the three LWAs are listed in Table 4. The calculated results are consistent with the measurement and simulation results. The simulated radiation efficiencies of the three LWAs are 45.5%, 47.5% and 43.6%. The measured radiation efficiencies of the three LWAs are 44 %, 45.6% and 41.5%. The axial ratios of the three LWAs are shown in Fig. 17. The proposed model has basically good performance and accuracy to predict the radiation properties of the annular LWAs based on

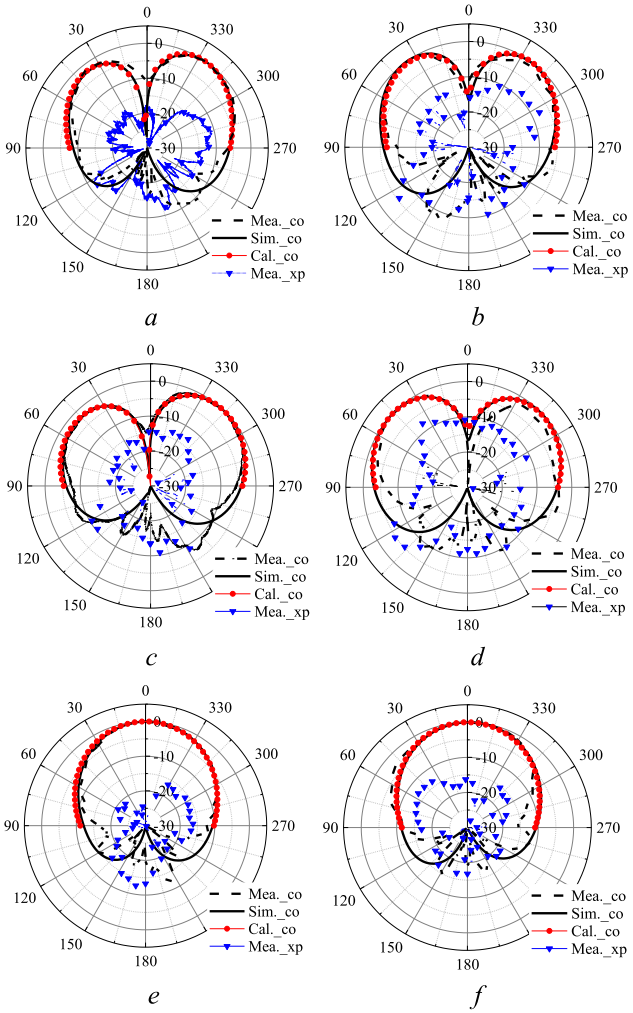

FIGURE 16. Radiation patterns of the LWAs: (a) LWA 1 in the *xoz*-plane, (b) LWA 1 in the *yoz*-plane (c) LWA 2 in the *xoz*-plane, (d) LWA 2 in the *yoz*-plane, (e) LWA 3 in the *xoz*-plane, (f) LWA 3 in the *yoz*-plane.

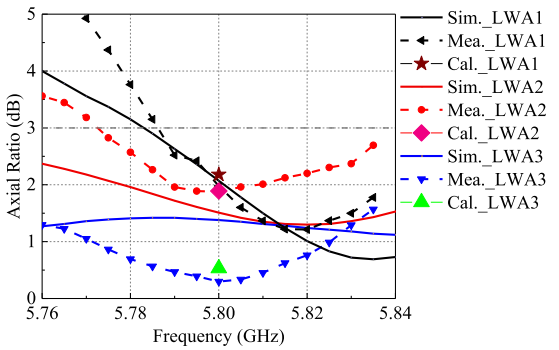

FIGURE 17. Axial ratio in the beam pointings of LWAs 1, 2 and 3.

the travelling-wave structure, which is a useful tool for the antenna design.

IV. CONCLUSION

In this paper, a theoretical model for the slotted annular LWA based on the travelling-wave structure is proposed. Radiating

elements are arranged along a circle with constant intervals. The model uses the aperture field of one single element to calculate the far field of the entire LWA. The conclusion is that the model can be used to efficiently predict the radiation pattern and axial ratio of the LWA. Using this model, design procedures of LWA with the desired CP conical beam or broadside beam can be simplified.

REFERENCES

[1] X. Bai, X. Liang, M. Li, B. Zhou, J. Geng, and R. Jin, "Dual-circularly polarized conical-beam microstrip antenna," *IEEE Antennas Wireless Propag. Lett.*, vol. 14, pp. 482–485, 2015.

[2] W. Lin, H. Wong, and R. W. Ziolkowski, "Circularly polarized antenna with reconfigurable broadside and conical beams facilitated by a mode switchable feed network," *IEEE Trans. Antennas Propag.*, vol. 66, no. 2, pp. 996–1001, Feb. 2018.

[3] C.-Y.-D. Sim, "Conical beam array antenna with polarization diversity," *IEEE Trans. Antennas Propag.*, vol. 60, no. 10, pp. 4568–4572, Oct. 2012.

[4] S.-S. Qi, W. Wu, and D.-G. Fang, "Singly-fed circularly polarized circular aperture antenna with conical beam," *IEEE Trans. Antennas Propag.*, vol. 61, no. 6, pp. 3345–3349, Jun. 2013.

[5] J.-S. Row and M.-C. Chan, "Reconfigurable circularly-polarized patch antenna with conical beam," *IEEE Trans. Antennas Propag.*, vol. 58, no. 8, pp. 2753–2757, Aug. 2010.

[6] W. Lin and H. Wong, "Circularly polarized conical-beam antenna with wide bandwidth and low profile," *IEEE Trans. Antennas Propag.*, vol. 62, no. 12, pp. 5974–5982, Dec. 2014.

[7] W. Lin and H. Wong, "Polarization reconfigurable wheel-shaped antenna with conical-beam radiation pattern," *IEEE Trans. Antennas Propag.*, vol. 63, no. 2, pp. 491–499, Feb. 2015.

[8] H. Xu, J. Zhou, K. Zhou, and Z. Yu, "Low-profile circularly polarised patch antenna with high gain and conical beam," *IET Microw., Antennas Propag.*, vol. 12, no. 7, pp. 1191–1195, Jun. 2018.

[9] S. Karki, M. Sabbadini, K. Alkhalifeh, and C. Craeye, "Metallic monopole parasitic antenna with circularly polarized conical patterns," *IEEE Trans. Antennas Propag.*, vol. 67, no. 8, pp. 5243–5252, Aug. 2019.

[10] D. Yu, S.-X. Gong, Y.-T. Wan, and W. Jiang, "Wideband conical-beam circularly polarized microstrip antenna for large ground plane," *IEEE Trans. Antennas Propag.*, vol. 63, no. 10, pp. 4614–4619, Oct. 2015.

[11] Y. Pan and K. W. Leung, "Wideband circularly polarized dielectric bird-nest antenna with conical radiation pattern," *IEEE Trans. Antennas Propag.*, vol. 61, no. 2, pp. 563–570, Feb. 2013.

[12] H. Xu, J. Zhou, Q. Wu, Z. Yu, and W. Hong, "Wideband low-profile SIW cavity-backed circularly polarized antenna with high-gain and conical-beam radiation," *IEEE Trans. Antennas Propag.*, vol. 66, no. 3, pp. 1179–1188, Mar. 2018.

[13] G. Chenhu, J. Geng, H. Zhou, J. Li, L. Liu, X. Liang, W. Zhu, R. Jin, and R. W. Ziolkowski, "Truncated circular cone slot antenna array that radiates a circularly polarized conical beam," *IEEE Antennas Wireless Propag. Lett.*, vol. 16, pp. 2574–2577, 2017.

[14] S. V. Kumar and A. R. Harish, "Generation of circularly polarized conical beam pattern using torus knot antenna," *IEEE Trans. Antennas Propag.*, vol. 65, no. 11, pp. 5740–5746, Nov. 2017.

[15] H. Nakano, H. Oyanagi, and J. Yamauchi, "A wideband circularly polarized conical beam from a two-arm spiral antenna excited in phase," *IEEE Trans. Antennas Propag.*, vol. 59, no. 10, pp. 3518–3525, Oct. 2011, doi: 10.1109/TAP.2011.2163759.

[16] B. Wen, Z.-H. Yan, K. Chen, and Y. Shi, "A low-profile two-arm Archimedean spiral antenna radiating a circularly polarized normal beam or conical beam," in *Proc. Int. Workshop Microw. Millim. Wave Circuits Syst. Technol.*, Chengdu, China, Oct. 2013, pp. 62–65.

[17] Y. Liu, M. Li, K. Song, D. Hu, H. Liu, X. Zhao, S. Zhang, and M. Navarro-Cia, "Leaky-wave antenna with switchable omnidirectional conical radiation via polarization handedness," *IEEE Trans. Antennas Propag.*, vol. 68, no. 3, pp. 1282–1288, Mar. 2020.

[18] S. J. Chen, C. Fumeaux, Y. Monnai, and W. Withayachumnankul, "Dual circularly polarized series-fed microstrip patch array with coplanar proximity coupling," *IEEE Antennas Wireless Propag. Lett.*, vol. 16, pp. 1500–1503, 2017.

[19] Y.-H. Yang, J.-L. Guo, B.-H. Sun, Y.-M. Cai, and G.-N. Zhou, "The design of dual circularly polarized series-fed arrays," *IEEE Trans. Antennas Propag.*, vol. 67, no. 1, pp. 574–579, Jan. 2019.

[20] D. Xie, L. Zhu, X. Zhang, and N. Liu, "Gain-enhanced EH_1-mode microstrip leaky-wave antenna with periodical loading of shorting pins," *IET Microw., Antennas Propag.*, vol. 12, no. 2, pp. 230–236, 2018.

[21] F. Xu and K. Wu, "Guided-wave and leakage characteristics of substrate integrated waveguide," *IEEE Trans. Microw. Theory Techn.*, vol. 53, no. 1, pp. 66–73, Jan. 2005.

[22] X. Li, J. Wang, Z. Li, Y. Li, M. Chen, and Z. Zhang, "Dual-beam leaky-wave antenna array with capability of fixed-frequency beam switching," *IEEE Access*, vol. 8, pp. 28155–28163, 2020.

[23] X. Zhang and L. Zhu, "Gain-enhanced patch antennas with loading of shorting pins," *IEEE Trans. Antennas Propag.*, vol. 64, no. 8, pp. 3310–3318, Aug. 2016.

[24] Y. Ma, J. Wang, Z. Li, Y. Li, M. Chen, and Z. Zhang, "Planar annular leaky-wave antenna array with conical beam," *IEEE Trans. Antennas Propag.*, vol. 68, no. 7, pp. 5405–5414, Jul. 2020.

[25] S. Mohaghegh Mohammadi, L. K. S. Daldorff, J. E. S. Bergman, R. L. Karlsson, B. Thide, K. Forozesh, T. D. Carozzi, and B. Isham, "Orbital angular momentum in radio—A system study," *IEEE Trans. Antennas Propag.*, vol. 58, no. 2, pp. 565–572, Feb. 2010.

[26] C. A. Balanis, "Leaky-wave antennas," in *Modern Antenna Handbook*. Hoboken, NJ, USA: Wiley, 2008, pp. 325–367.

YUCHEN MA was born in Beijing, China, in 1993. He received the B.E. degree from the School of Electronic and Information Engineering, Beijing Jiaotong University, Beijing, China, in 2015, where he is currently pursuing the Ph.D. degree with the Institute of Lightwave Technology.

His current research interest includes smart antenna based on multi-physical-quantity acquisition.

JUNHONG WANG (Senior Member, IEEE) was born in Jiangsu, China, in 1965. He received the B.S. and M.S. degrees in electrical engineering from the University of Electronic Science and Technology of China, Chengdu, China, in 1988 and 1991, respectively, and the Ph.D. degree in electrical engineering from Southwest Jiaotong University, Chengdu, in 1994. In 1995, he joined as a Faculty Member with the Department of Electrical Engineering, Beijing Jiaotong University, Beijing, China, where he became a Professor, in 1999. From January 1999 to June 2000, he was a Research Associate with the Department of Electric Engineering, City University of Hong Kong, Hong Kong. From July 2002 to July 2003, he was a Research Scientist with Temasek Laboratories, National University of Singapore, Singapore. He is currently with the Key Laboratory of all Optical Network and Advanced Telecommunication Network, Ministry of Education, Beijing Jiaotong University, and the Institute of Lightwave Technology, Beijing Jiaotong University. His research interests include numerical methods, antennas, scattering, and leaky wave structures.